PERGAMON

Journal of Structural Geology 22 (2000) 571–588

JOURNAL OF STRUCTURAL GEOLOGY

www.elsevier.nl/locate/jstrugeo

Prediction of macrofracture properties using microfracture information, Mesaverde Group sandstones, San Juan basin, New Mexico

Orlando Ortega*, Randall Marrett

Department of Geological Sciences, University of Texas at Austin, Austin, TX 78712, USA

Received 15 March 1999; accepted 10 December 1999

Abstract

A better understanding of relationships between microfractures and macrofractures is prerequisite to the extrapolation of observed microfracture properties as a basis for inferring properties of associated macrofractures. The hypothesis that micro- and macrofractures represent different size fractions of the same fracture sets, and consequently have linked attributes, was tested on sandstones of the Mesaverde Group, San Juan basin, New Mexico. The use of a cathodoluminescence detector attached to a Scanning Electron Microscope (SEM) allowed observation of microfractures not readily visible using conventional microscopic techniques.

The orientations of microfractures reproduce the orientations recorded at the macroscopic scale from cores and outcrops. Fracture size distributions are best modeled using power laws, and extrapolation of microfracture frequencies to the scale of macrofractures successfully predicts the macrofracture frequencies. Fracture-size distributions change at the length scale of the thickness of the mechanical layer, typically by increasing the exponent of their power-law distribution. This change is independent of censoring biases and reflects changes in sampling topology and/or fracture growth mechanisms.

1. Introduction

Fractures are important fluid-flow conduits in the subsurface and important repositories of economic mineral resources. Analysis of core samples provides the most direct method to sample fractures in the subsurface. However, cores provide a volume of rock that is too small to characterize large fractures, which commonly have dimensions and spacing that are larger than the diameter of core (Laubach, 1988). In contrast, microfractures are usually more abundant than the associated macrofractures in the same volume of rock (Laubach and Milliken, 1996; Ortega, 1997) and abundant data about their dimensions and spatial distribution can be systematically recorded from small samples. Thus, scaling methods can potentially solve fracture-sampling problems by using complete fracture data sets at the microscopic scale and extrapolating this information to the macroscopic scale.

The extrapolation of fracture characteristics across many orders of magnitude in size is fraught with potential danger. For example, many different types of mechanical discontinuities, such as bed and grain boundaries, affect fracture growth in sedimentary rocks (e.g. Corbett et al., 1987; Laubach, 1997). Yet the orientation of micron-scale fractures is consistent with the orientation of meter-scale fractures in some sandstones (Laubach, 1997), suggesting that at least under some circumstances the extrapolation of fracture attributes from the microscale to the macroscale is justified.

Several authors have shown that open-mode fracture systems are organized such that their size dis-

* Corresponding author.
E-mail address: o.ortega@mail.utexas.edu (O. Ortega).

0191-8141/00/$ - see front matter
PII: S0191-8141(99)00186-8

tributions follow power-laws (Gudmundsson, 1987; Wong et al., 1989; Heffer and Bevan, 1990; Barton and Zoback, 1992; Gillespie et al., 1993; Hatton et al., 1994; Sanderson et al., 1994; Belfield and Sovich, 1995; Clark et al., 1995; Gross and Engelder, 1995; Johnston and McCaffrey, 1996; Marrett, 1997). However, deviations from a simple power-law relationship by the smallest and largest observed fractures are common. Truncation and censoring sampling biases commonly explain these deviations (Baecher and Lanney, 1978; Laslett, 1982; Barton and Zoback, 1992; Pickering et al., 1995), but sampling topology (Marrett and Allmendinger, 1991; Marrett, 1996) and rock heterogeneity (Wojtal, 1994; 1996) might similarly affect observed fracture-attribute scaling. A better understanding of these observed deviations is needed to determine the limitations of extrapolation across different scales and material boundaries. Furthermore, systematic changes in fracture size distributions might be predicted, modeled and/or ignored for extrapolation purposes.

This study attempts the first systematic investigation of extrapolation of microscopic fracture data to predict quantitatively macroscopic fracture properties. Microfracture data can be collected systematically from small areas (few mm^2) of a thin section using CL devices. However, in many sedimentary siliciclastic rocks a cathodoluminescence detector attached to a scanning electron microscope (SEM-CL) is needed to resolve most of these small structures (Laubach and Milliken, 1996; Laubach, 1997 and references therein). If reliable predictions of macrofracture characteristics are possible based on microscopic data, then small oriented samples will augment understanding of the orientation, size, frequency and timing of associated macrofractures. This is important because beds with different composition, diagenesis or thickness often show different fracture frequencies and even different fracture orientations. The prediction of which beds are more likely to have large fractures, and what orientations and spatial frequencies those fractures have, carries important economic implications and yields insight on how fractures develop in buried rocks.

Sandstones of the Mesaverde Group (Upper Cretaceous) in the San Juan basin, New Mexico, were selected to study the feasibility of extrapolation of microfracture properties to macrofractures because excellent outcrops expose these units along the basin margins and active petroleum exploration for fractured reservoirs provide opportunities for studying subsurface samples. Consequently, high quality micro- and macrofracture data, from surface and subsurface, can be collected from this sedimentary sequence.

2. Regional and local settings

The San Juan basin is located in the Colorado Plateau and contains a column of more than 5000 m of Paleozoic to Tertiary sedimentary rocks. Structural contours of the basin at Cretaceous and younger levels indicate that strata are unaffected by major folds or faults. The borders of the basin show more complex structural features such as the Hogback monocline, Nacimiento uplift and Archuleta uplift (Fig. 1). The fracture systems of the San Juan basin have been studied by a number of authors (Kelley and Clinton, 1960; Gorham et al., 1979; Condon, 1988, 1989; Laubach and Tremain, 1991; Dart, 1992; Huffman and Condon, 1993) who primarily focused on description of the macroscopic fracture systems in different parts of the basin and in a variety of stratigraphic units.

The Mesaverde Group is a major regressive–transgressive cycle in the filling history of the basin during the Late Cretaceous. Shales and sandstones dominate the sedimentary sequence of the Mesaverde Group. Some sandstone members of the Cliff House, Menefee and Point Lookout Formations have long been recognized as fractured hydrocarbon reservoirs (e.g. Hollenshead and Pritchard, 1961). In order to study fractures in these units, we collected surface data from two gently dipping sandstone bedding plane pavements (Westwater and Cottonwood areas, Fig. 1 and Table 1) and from three oriented cores of the same stratigraphic units in the Blanco–Mesaverde gas field (Fig. 1; Table 2).

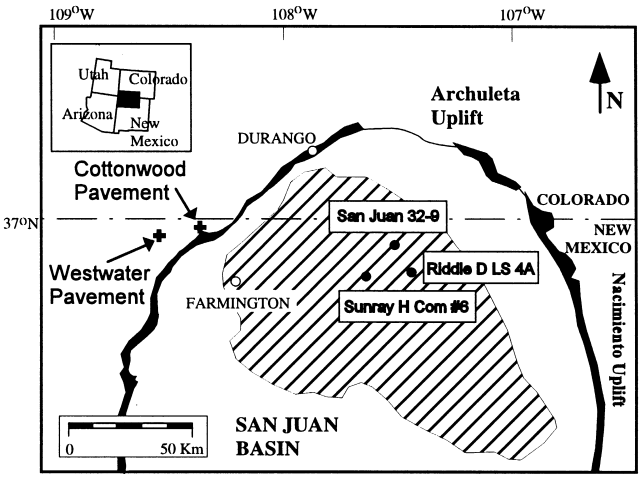

Fig. 1. Location map of pavements and wells. The San Juan basin is the area surrounded by the Hogback monocline (black), a topographic feature around the basin containing outcrops of weather resistant units of Cretaceous and Tertiary age. Hatched area represents gas fields included in the Blanco–Mesaverde giant gas accumulation. The inset in the upper-left corner shows the location of the study area in the context of the Four Corners Area.

Table 1
Mesaverde sandstone pavement characteristics

Pavement	Formation	Bedding Dip	Small Area (m^2)	Large Area (m^2)	Number of Samples
Westwater	Point Lookout	5°	2069	13365	17
Cottonwood	Cliff House	10°	2034		18

2.1. Sandstone texture and diagenesis

The sandstones analyzed are medium to very fine grained. The degree of compaction is low, as indicated by the predominance of point contacts between the grains, except in the Sunray H Com ♯6 well where the core shows abundant bed-parallel stylolites. According to Folk's (1980) classification, the sandstones are sublitharenites and litharenites (Ortega, 1997). The subsurface rocks have low permeability, in general less than 1 md, and porosities less than 5% (Weir, 1996). The same stratigraphic units in outcrops are more porous (3–15%) than their subsurface equivalents. This result reflects differences in the degree of mechanical compaction and differences in the volume of carbonate cement (5–10% of rock).

Diagenetic processes had variable volumetric effects in the different units analyzed but the sequence of events was the same in all cases (Fig. 2). The lack of evidence for significant grain-to-grain interpenetration suggests that authigenic quartz precipitated relatively early. SEM-CL images show that the quartz in overgrowths and that filling post-depositional fractures have the same luminescence. This observation probably indicates that microfracturing was partially synchronous with quartz overgrowths. Carbonate cement filled primary porosity left by quartz overgrowths, suggesting it precipitated later. Fracture fill also shows these timing relationships, as confirmed by crack–seal quartz cement in macrofractures (synkinematic cement; Laubach et al., 1995) and carbonate cement filling spaces between quartz lined fracture walls (postkinematic cement; Laubach et al., 1995).

3. Observational and analytical methods

The limitations to fracture observation differ significantly between microscopic and macroscopic scales and also between natural exposures and subsurface cores. In this study, macrofractures are defined to be those fractures visible with the unaided eye; smaller fractures are considered to be microfractures (Laubach, 1997). Macrofracture data were chiefly collected by visual inspection of outcrops and cores. Microfracture data were collected from thin sections using petrographic and scanning electron microscopes.

3.1. Macrofracture data from cores

The description of the macrofractures present in cores included: depth, height, mechanical aperture, strike, dip, and types of mineral fill in the fracture, if any. All natural fractures, whether open, partly-open or filled, were measured. Natural and drilling-induced fractures were distinguished based on the presence of mineral fill of cement lining natural fractures or distinctive drilling-induced fracture shapes (Kulander et al., 1990).

Macrofracture orientations for the wells were obtained from oriented core and from image logs. The dip of most macrofractures is nearly vertical, so only macrofracture strike was recorded in most cases. Macrofracture lengths cannot be obtained in the majority of cases due to lengths exceeding the core diameter. Minimum values of fracture height were measured in most instances due to fractures extending beyond the core volume. This sampling problem limits the reliability of macrofracture-height distributions from core.

The measurement of macrofracture apertures was done using gauges, rulers and magnifiers and includes the width of any remnant porosity and mineral filling of the fractures. Broken fractures, ones with walls no longer held together by mineralization, are abundant in cores and no reliable estimate of the fracture

Table 2
Mesaverde sandstone core characteristics

Well	Formation	Core Length (m)	Number of samples	Method of Orientation
Riddle D LS 4A	Cliff House	17.5	22	Inclined Well
Sunray H Com ♯6	Cliff House	13.1	15	Magnetic
San Juan 32-9	Cliff House	21.5	1	Image Log
	Meneffe	11.8	6	Image Log
	Point Lookout	23.5	5	Image Log

aperture can be obtained. Only a minimum fracture aperture can be estimated from the thickness of the remaining cement on the broken surfaces of such a fracture.

Fracture cements can be categorized according to when they precipitated relative to fracture opening (Laubach, 1988, 1997). Cementation/opening timing is established on the basis of cement texture and crosscutting relationships between the fractures and the cement phases identified in the rock. The percentages by volume of prekinematic, synkinematic and postkinematic cements in the rock were represented in a triangle diagram.

3.2. Macrofracture data from outcrops

The exposure of fracture systems in sandstone pavements of the Mesaverde Group allowed the collection of more complete data on fracture sizes than from the cores. Scattered lichen patches cover the top of the exposed sandstone surfaces and limit the visibility of macrofractures shorter than approximately 10 cm long. On the other hand, weathering helps the detection of fractures due to the contrast in weathered color and resistance to erosion between the fracture fill and the host rock.

Particularly well-exposed areas within the pavements were selected to catalogue open-mode macrofracture properties. Surveys around these areas were carried out to calculate the surface area of observation for derivation of fracture frequencies (Table 1). The selection of different size observation areas in Westwater pavement allowed data collection at different resolutions. From the large observation area (13,365 m^2) only fractures longer than the thickness of the mechanical layer were recorded, whereas from the small area (2060 m^2) all the fractures visible with the naked eye were measured.

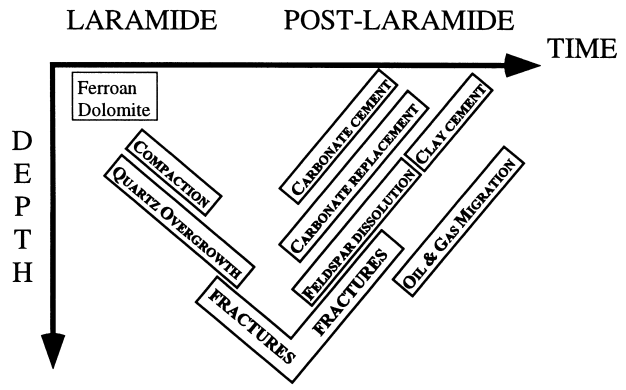

Fig. 2. Schematic paragenetic sequence for Mesaverde Group sandstones. Fractures probably formed during burial and subsequent uplifting. Timing is based on crosscutting relationships between fractures, cement and dissolution/replacement events. Gas migration and schematic burial history are taken from Bond (1984).

In outcrop, fracture length measurement is complicated by the challenge of defining what constitutes an individual fracture where multiple fracture strands connect. The best approach to measuring the length of a fracture is to use criteria that uniquely identify fracture terminations, as will be discussed in detail below. Fracture length data were also collected along scanlines on Westwater pavement. The purpose of the one-dimensional data was to test the approach of estimating two-dimensional fracture distributions using scanline data (Marrett, 1996).

In addition to two-dimensional sampling of fracture lengths, two-dimensional fracture heights were also collected along the Westwater Springs canyon walls for fracture length–height comparison. The analysis of fracture-height distribution and its comparison with the fracture length data obtained from the pavements allowed us to make inferences about the geometry of the fracture surfaces and the influence of fracture geometry on fracture-size distributions.

Fracture apertures were difficult to measure in the field because the fracture aperture, filled with quartz and carbonate minerals, is usually surrounded by a fracture skin of carbonate-cemented sand grains in which the exact location of the walls of the fracture are unclear even under magnification.

3.2.1. Fracture terminations

No specific criteria have been proposed to determine uniquely the lengths of interconnected fractures. Below are the criteria used in this study, in descending order of applicability:

1. At the branch point of three connected fracture segments, the two segments having the most similar apertures constitute a through-going fracture and the third segment represents a different fracture with a termination at the connection point.
2. At the branch point of three connected fracture segments, the two segments having continuous fracture filling characteristics constitute a through-going fracture and the third segment represents a different fracture with a termination at the connection point.
3. At a branch point of three connected fracture segments, the two segments having the most similar strike constitute a through-going fracture and the third segment represents a different fracture with a termination at the connection point.

3.2.2. Fracture connectivity

Connectivity is a fundamental property of fracture systems in terms of fluid flow. The quantification of this parameter would allow comparison of different

fracture networks and modeling of fluid flow through fracture systems in ways that are more realistic than commonly used. Establishing relationships between more readily measurable fracture attributes and connectivity will help to predict quantitatively the connectivity of fracture networks in the subsurface, which cannot be observed directly.

The connectivity of a fracture system has different meanings in mechanical and hydrodynamical contexts. The mechanical connectivity of fractures focuses on the degree of physical connection among the fractures in a network. On the other hand, in fluid flow applications, some fractures can be physically connected to a network but isolated in the sense that the connections are nonconductive to flow (e.g. mineral filled fractures). The hydrodynamic connectivity of fractures is affected by chemical factors in addition to physical ones.

In this work, a new approach was taken to characterize connectivity semi-quantitatively. This method takes into account the number of fractures with two or more connections, one connection or no connections in the system and the number of fractures in the entire system (Fig. 3). The proportion of connection (null, single or multiple) is given by the ratio of the number of fractures in the population that are isolated (Type I), singly connected (Type II) or multiply connected (Type III) with respect to the total number of fractures, and can be illustrated using a triangle diagram. This approach is similar to Laubach's (1992) approach but replaces the 'constricted' fractures with fractures having only one connection to another fracture. This method also complements Robinson's (1983) approach to quantitative characterization of fracture connectivity, which does not differentiate fractures with a single connection (Type II), from multiply connected fractures (Type III). The distinction between these two kinds of fractures is particularly important for the analysis of fluid-flow through fracture systems.

As Laubach (1992) pointed out, the connectivity of fracture networks is a scale dependent parameter because small 'invisible' fractures can connect large fractures. A first-order evaluation of fracture connectivity can be achieved by restricting attention to macroscopic fractures.

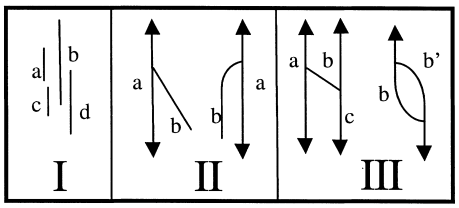

Fig. 3. Fracture termination types observed in the field. Isolated fractures (Type I, e.g. fracture b), singly connected fractures (Type II, fracture b), and fractures connected with other fractures in more than one place (Type III, fractures b, b').

3.2.3. Mechanical layer thickness

An estimate of the thickness of the mechanical layer examined at each pavement was determined by studying the fracture system in cross-section along canyon walls. The definition of a mechanical layer is based on the stratigraphic consistency of upper and lower fracture terminations within a bed or group of beds (Corbett et al., 1987; Helgeson and Aydin, 1991; Gross, 1993). Often, significant changes in fracture frequency distinguish the limits of a mechanical layer. These differences in fracture frequency can be controlled by compositional or depositional facies variation, authigenic cement distribution, porosity or a combination of these and other factors at the time when fractures formed (Laubach et al., 1995). In some cases the mechanical differences between the layers also correlate with differences in their weathering.

3.3. Microfracture data

Microfracture data were collected from both subsurface and surface oriented samples. Based on observations in other formations (Laubach, 1997), we assumed that most microfractures related to macrofractures in the Mesaverde Group form high angles with stratification, as do macrofractures. Thus, thin sections were cut parallel to stratification, providing microscopic views comparable to the two-dimensional macroscopic outcrops.

The thin sections were polished with aluminum and covered with a carbon coating (dark blue degree) for study under the SEM-CL. The methodologies to image microfractures included: random photomicrographs throughout the thin section, systematic transects in predefined orientations and/or mosaics covering small portions of the thin section. Standard operating procedures are described in Milliken (1994). Magnification values were set on the order of 200× for general microfracture detection and 500× to define details of fracture morphology or fracture/cement relationships. The Energy Dispersive X-ray Spectrum device allowed the determination of the composition of microfracture fill.

The use of SEM-CL allowed observation of microfractures not readily visible using conventional microscopic techniques (Laubach, 1997). Fracture length, maximum mechanical aperture and fracture strikes were determined for each microfracture in the photographs (Ortega, 1997). A grading scheme derived from Laubach's (1997) descriptive classification was used to assign a rank to the microfractures based on the morphology of microfractures and the relationships of microfractures with grains, cement, and other

microfractures (Table 3). This ranking refers to the predictive value (suitability) of a microfracture for purposes of macrofracture characterization, according to the interpreted likelihood that a microfracture is a product of the same processes that generated the macrofractures. Microfracture suitability is a genetic alternative to the term 'reliability' in Laubach's (1997) descriptive classification.

In some instances, the SEM-CL cannot illuminate the details of microfracture morphology necessary to classify microfractures. For example, the presence of highly luminescent minerals in the rock adversely affects image quality. Such limitations added uncertainty to microfracture classification for some samples. Also, the recognition of microfracture continuity is complicated by difficulties in distinguishing certain segments of microfractures. For example, some microfractures may follow grain boundaries, where they can apparently terminate against pores, or they can simply be difficult to distinguish from intergranular cement.

3.4. Analyses of fracture data

3.4.1. Fracture orientation

Rose diagrams of micro- and macrofracture strike were made for comparison. Several different approaches were taken to analyze the microfracture orientation data. All microfracture orientations from each sample were initially plotted and compared with the associated macrofracture orientations. In some cases the preferential orientation of all of the microfractures in a sample corresponds with the orientation of the macrofractures developed in the same bed. In cases in which the orientations of all of the microfractures differed from or were more complex than the macrofracture orientations, comparisons were made between the macrofracture orientations and the orientations of increasing suitability microfractures. Additionally, and in order to avoid the subjective component introduced by the ranking scheme, the microfracture orientations were weighted according to lengths. The length-weighting procedure consists of repetition of the fracture strike for every 10 μm of fracture length. In this way the longest fractures (i.e. the ones that are most likely to be transgranular or transcement) have the most influence on the microfracture orientations.

3.4.2. Fracture size distribution

Cumulative frequency distributions were obtained by normalizing the cumulative fracture-size distribution by the size of the observation domain. Cumulative frequency fracture-size distributions are best illustrated using log–linear and log–log graphs. Lines can be fit to linear trends of data points in both types of graphs implying that either exponential or power (fractal) laws, respectively, can be used to model fracture-size distributions. Different authors have supported one or the other type of distribution with particular data sets (negative exponential: Snow, 1970; Baecher et al., 1977; power-law: Gudmundsson, 1987; Wong et al., 1989; Heffer and Bevan, 1990; Barton and Zoback, 1992; Hatton et al., 1994; Sanderson et al., 1994; Belfield and Sovich, 1995; Clark et al., 1995; Gross and Engelder, 1995; Johnston and McCaffrey, 1996; Marrett, 1997). No model typically fits entire data sets, a result that commonly is interpreted to reflect various sampling limitations. The possible causes of artifacts in the fracture size distributions were also analyzed. Censoring bias is produced by incomplete measurements of the longest fractures, because they extend beyond the limits of the area studied. Truncation bias is associated with increasing difficulty of detection for progressively smaller fracture sizes (Baecher and Lanney, 1978; Barton and Zoback, 1992; Pickering et al., 1995). The difficulties of uniquely recognizing the tips of individual fractures

Table 3
Microfracture classification

Suitability	Characteristics	Laubach (1997) (see Fig. 3)	Genetic interpretation
A (high)	Filled transgranular and transcement microfractures	Ia+, Ia	Post-depositional, Post-cementation
B (medium)	Microfractures filled with same cement surrounding the grains and in physical continuity with cement	some Ib, Ic, Id	Post-depositional, Pre/Syn-cementation
C (low)	Microfractures in net-like arrays, grain restricted, with radial orientations, variable apertures, and irregular traces. Microfractures at the borders or tips of grains. Microfractures that do not cut a whole grain. Open microfractures with no mineralization	II and some Ib, Ic, Id	Post-depositional. Grain crushing related. Produced by local stress concentration at borders or tips of grains. Possibly induced fractures
D (none)	Microfractures filled with cement not found around grains. Usually diffuse or with odd traces	III, and some Ic, Id	Pre-depositional

where multiple fracture strands connect introduces a non-systematic bias, which requires the definition of criteria for cataloging fracture length (see Section 3.2.1).

In order to avoid subjective treatment of data sets, selection of the model that best describes a fracture size distribution should be based on application of systematic error analysis. This procedure also helps to determine which part of a data set should be used to obtain the model that best describes the data. A parameter that measures error for least-squares regression is the correlation coefficient (r). The value of r^2 has been calculated on equal footing for both exponential and power-law regressions to the distributions. An example of the application of this methodology is left for the Section 4, but here we provide a summary of the steps involved in the analysis:

1. The coefficient of determination (r^2) is calculated for the least-squares regression to the three smallest fracture sizes in the cumulative frequency size distribution, considering both the exponential and the power-law models. This parameter (r^2) is recalculated including the next larger fracture size in the distribution. The procedure is repeated adding progressively larger fracture sizes until the largest fracture size of the distribution has been included in the calculation. Similarly, this procedure is applied starting with the three largest fracture sizes and continued by adding progressively smaller fracture sizes and recalculating the squared correlation coefficient.
2. The results of the calculation of r^2 can be analyzed in a graph showing the variation of r^2 as a function of the range of fracture sizes considered. The model that best explains the observations shows the highest r^2 values for the corresponding range of fracture sizes. Significant inflection points in the r^2 curves indicate fracture sizes where a particular model starts to depart significantly from the observations. These points determine the limits of the distribution to be used for the interpretation of the model parameters that best describe the observations.

3.4.3. Fracture cementation timing

The analysis of fracture-cementation timing relative to fracture opening and the volumetric proportions of different categories of cement in the rock (Laubach, 1988, 1997) helps characterize the degree of occlusion of fractures and provides information about the relative capacity of fractures to conduct fluids. Prekinematic cements cannot occlude fractures, but result in reduced matrix porosity. Postkinematic cements reduce fracture permeability and occlude matrix porosity, decreasing the potential of the rock for fluid flow (Laubach et al., 1995). Synkinematic cements can produce the same results as postkinematic cements if pervasive, but commonly this type of cement only partially fills fracture space. The presence of mineral bridges in partially filled fractures prevents fracture closure and preserves fracture permeability (Marrett and Laubach, 1997).

4. Results

4.1. Fracture sets and cross-cutting relationships

Three distinct natural fracture systems were identified in outcrops of the Mesaverde Group: shear-mode conjugate fractures (faults), open-mode sealed fractures (veins) and open-mode surface-related fractures (joints and polygonal cracks). Joints are open-mode fractures interpreted to be associated with the release of confining pressure of buried rocks exposed to the surface and/or the action of gravity at cliff borders or slopes. Polygonal cracks are open-mode fractures interpreted to form by rock dilation due to changes in temperature. The surface-related fracture systems observed in the outcrops will not be further discussed in this paper because we focused our attention on fracture systems present both in outcrop and in the subsurface.

Shear fractures were recognized only in outcrops and not in cores. Shear fractures are commonly rectilinear and consist of two mutually crosscutting sets of conjugate strike-slip faults forming acute angles of 70–25°. The shear fractures are characterized by the presence of cataclasite.

Open-mode mineralized fractures observed in the outcrops are typically grouped in swarms. They show more sinuous traces and crosscut the older shear-mode fractures. Hooked connections between fractures suggest open-mode propagation under nearly isotropic remote stresses (Olson, 1993).

Natural macrofractures in core were difficult to identify, in part due to the lack of obvious mineralization on the surfaces of most fractures, but also due to the limited amount of material available for study. Natural fractures in the inclined Riddle D LS 4A well typically intersect bedding at high angle. In the core of the Sunray H COM ♯6 well, natural fractures show en échelon arrangement. The cores from the San Juan 32-9 well show natural mineralized fractures. The morphologic differences of the open- and shear-mode macrofractures under the petrographic microscope are distinctive. Euhedral crystals typically line open-mode natural fractures.

4.2. Fracture cementation

The outcrops and cores show differences in macrofracture cement volume and mineralogy. Fractures of

the Riddle D LS 4A and Sunray H Com ♯6 wells are partially filled with euhedral quartz whereas samples collected from outcrops and the San Juan 32-9 well show macrofractures lined with quartz and later filled by carbonate cement.

Qualitative differences in macrofracture opening and cement timing can be recognized in samples from the surface and subsurface in this study (Fig. 4). Cements in the Riddle D LS ♯4A and Sunray H Com ♯6 wells are predominantly prekinematic quartz and less importantly synkinematic quartz, which lines fractures. The San Juan 32-9 well also shows prekinematic quartz cement, but synkinematic quartz overgrowths (~40%) and postkinematic carbonate cement (0–60%) are present in significant volumes. Postkinematic carbonate cements fill dominantly the macrofractures in outcrop samples.

Most of the microfractures in all samples are sealed by synkinematic cement. Most microfracture cements were contemporaneous with quartz overgrowth (95%) and fewer (5%) were synchronous with later carbonate precipitation.

4.3. Fracture connectivity

Isolated fractures and singly connected fractures (Fig. 5) dominate the connectivities of open-mode macrofracture swarms studied in the field. As a result, the total connectivity of the open-mode fractures is low in spite of their occurrence in swarms.

Map traces of microfractures from outcrop and core samples analyzed under the SEM-CL show that most of the microfractures are isolated. This implies that their physical connectivity is smaller than that of the macrofractures in the same rock volume. However, some grain boundaries are potential connecting conduits that we cannot readily identify in the photographs. This limitation makes it difficult to compare fracture connectivity at different observational scales.

The hydrodynamic connectivity is low in microfractures of the Cliff House Formation, both from outcrops and from cores, not only due to poor physical connectivity but also due to the fractures being almost completely filled with quartz cement. The macrofractures instead show proportionally lower cement volume and a greater degree of effective hydrodynamic connectivity. Core samples from the Point Lookout Formation show macrofractures lined with quartz cement and subsequently filled with carbonate cement. Almost all the microfractures in these samples are filled with quartz cement only. These observations suggest that the hydrodynamic connectivity and the proportions of cements filling the fractures vary with fracture size.

4.4. Microfracture and macrofracture orientations

Macrofracture strike is preferentially north to north-northeast in the Riddle D LS 4A and San Juan 32-9 wells (Fig. 6). The Sunray H Com ♯6 well has a preferential fracture strike of 60–90°. Conjugate shear fractures in both Westwater and Cottonwood pavements strike east (right slip) and northwest (left slip) suggesting that the maximum shortening axis was oriented WNW during faulting. The open-mode sealed fractures show constant 10–30° strike in both pavements. This orientation is consistent with a WNW-trending maximum horizontal extension direction and inconsistent with the orientation of the shortening axis of the conjugate faults, indicating that the shear and extension fractures formed at different times. This confirms the observed crosscutting relations.

High suitability microfractures (suitability A, Table 3) are preferred to determine microfracture strike for macrofracture prediction purposes, because they are most likely to have formed under the same

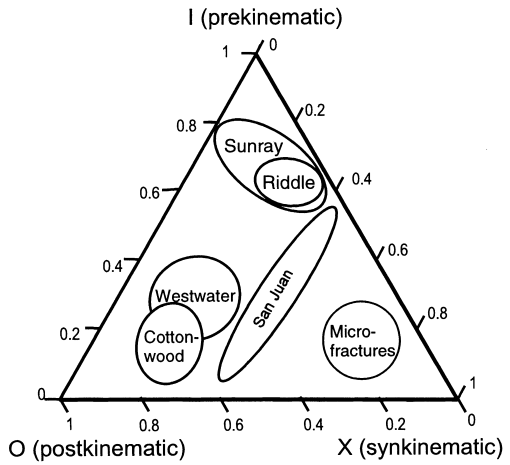

Fig. 4. Cement timing relative to fracture opening.

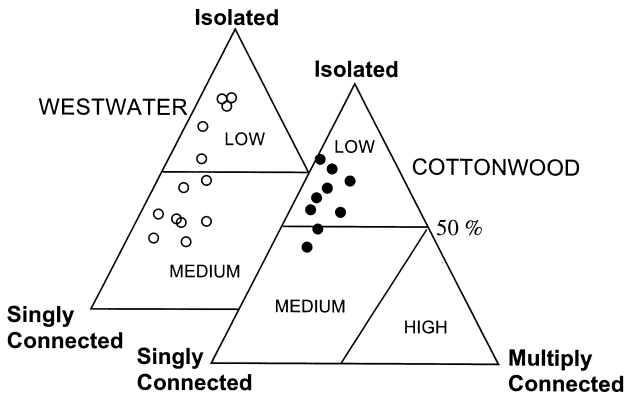

Fig. 5. Connectivity of fracture swarms in pavements studied. See Fig. 3 for definition of connectivity.

remote stress conditions as the macrofractures. The highest suitability fractures are the least common in the thin sections studied. After taking about 20 SEM-CL photomicrographs of a thin section (approximately 5 mm^2 at 200× magnification), at most 30 suitability C or higher microfractures could be identified. Of these fractures, usually less than 10% (i.e. three microfractures) can be classified as transgranular or transcement (suitability A). This small number of microfractures is insufficient to determine preferred orientations with high confidence.

The microfracture orientation analysis for data collected from five thin sections of samples from the San Juan 32-9 and Sunray H Com ♯6 wells and from outcrops are representative of the results overall (Ortega, 1997), in which a total of 26 samples were analyzed (Fig. 7). The Point Lookout Formation sample from the San Juan 32-9 well shows microfracture orientations in excellent agreement with the macrofracture orientations. In contrast, in the same well, the Menefee Formation sample shows high microfracture-orientation dispersion and the orientation of the macrofractures only appears clearly in the high suitability microfractures. Many intragranular fractures are present in this sample, adding to the diversity of the orientations of the less reliable microfractures. An additional set of east–west oriented microfractures in the Menefee Formation sample has no macrofracture equivalent in the core. However an east–west oriented macrofracture set is present in cores of the Sunray H Com ♯6 well (Fig. 6A).

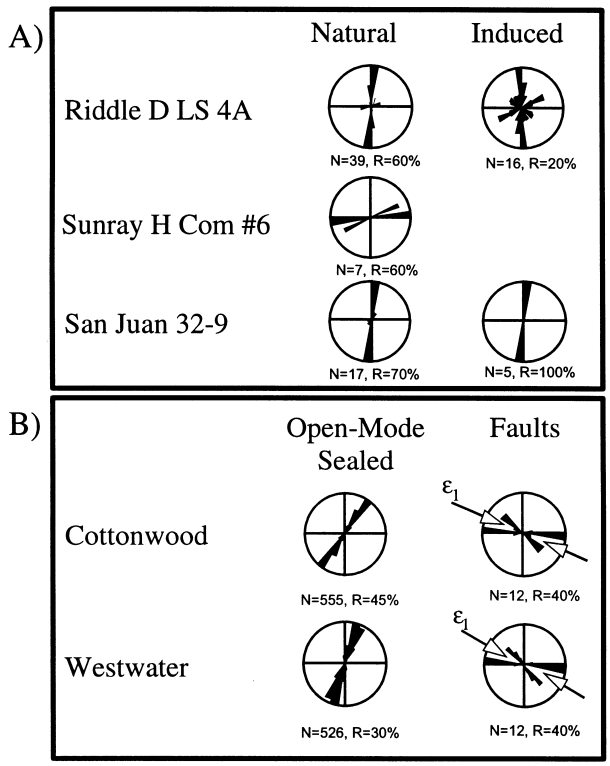

Fig. 6. Macrofracture strikes from cores (A) and outcrops (B) of Mesaverde Group sandstones. *N* is the number of macrofractures measured; *R* indicates approximate size (as a percentage of the total fracture population) of largest petal in rose diagrams; ϵ_1, is the interpreted horizontal projection of the maximum principal shortening direction for the conjugate fault systems, inferred from kinematic data.

The sample analyzed from the Sunray H Com ♯6 well exemplifies another kind of microfracture-orientation behavior. Although only seven macrofractures were observed in the core from this vertical well (Fig. 6A), they show similar east–west strikes. Near a swarm of four of these fractures, a sample was collected for microfracture analysis. In contrast with the adjacent macrofractures, the rose diagram of high suitability microfracture orientations shows a north–south strike (Fig. 7). This result agrees with the regionally predominant macrofracture orientation as seen in other wells. Due to the poor sampling of vertical fractures obtained from a vertical borehole, it is possible that north–south-striking macrofractures predominate even near this well and that the east–west-striking fractures represent only a local anomaly. In such a case, analysis focused solely on the few macrofractures encountered would lead to erroneous interpretation. However, even in the vicinity of such local structural anomalies, this result suggests that the regionally predominant fracture orientation can be correctly inferred from microfractures.

Outcrop samples also show interesting microfracture orientations when compared with the macrofractures. In the Cottonwood sample a strong northwest microfracture strike is produced by a few long microfractures (Fig. 7). This orientation is parallel to the shortening direction associated with the shear-mode fractures (Fig. 6B). The rest of the microfractures show a preferred NNE strike, aligned with the open-mode macrofracture system. A Westwater sample was intensively studied from a mosaic of SEM-CL photographs. Microfracture strikes in this sample correspond very well with the strike of the open-mode macrofractures. In summary, the comparison of strikes between micro- and macrofracture from five samples yielded three positive results and two indeterminate results.

In the cores of the Riddle D LS 4A well micro- and macrofracture strikes were compared in several beds because most of the core was oriented. In this well, the macrofractures have a consistent north–south strike (Fig. 6A). Most of the samples analyzed showed microfracture orientations similar to the macrofracture orientations. However, high suitability microfracture data collected from some samples was insufficient to compare adequately with macrofracture orientations.

A test carried out with one sample from the Riddle D LS 4A well explored the effects on the prediction of

macrofracture strike due to the amount of data available and the plotting technique used. The rose diagrams in Fig. 8A were obtained from the first 17 microfractures observed (representing approximately 3 mm^2 of the thin section). No satisfactory results were obtained from this data set. After observing 34 additional microfractures (an additional observation area covering approximately 8.5 mm^2), the results were still not satisfactory but represent some improvement over the initial attempt (Fig. 8B). Length weighting the collective group of 51 microfracture data (Fig. 8C) shows two preferential strikes: north–south and east–west. These correspond with the preferential orientations of macrofractures in this well (Fig. 6A).

This test suggests that additional data collected from other samples in this well could have further enhanced the agreement between macrofracture and microfracture orientations. Additionally, these results suggest that length weighting might minimize the need for a classification scheme, in some cases, in order to obtain the orientation signal of the macrofractures as long as sufficient data are collected.

4.5. Fracture size distributions

4.5.1. Effect of mechanical layer thickness on fracture scaling

On the Westwater pavement, fractures having lengths greater than the mechanical layer thickness ('long' fractures) are relatively sparse. These long fractures were best sampled in the large observation area, in which only fractures longer than the mechanical layer thickness were studied. Data from the long fractures are well modeled by a power law (Fig. 9A). In this case, all available data were used to calculate the power-law regression.

Fractures having lengths less than the mechanical layer thickness ('short' fractures) of the Westwater

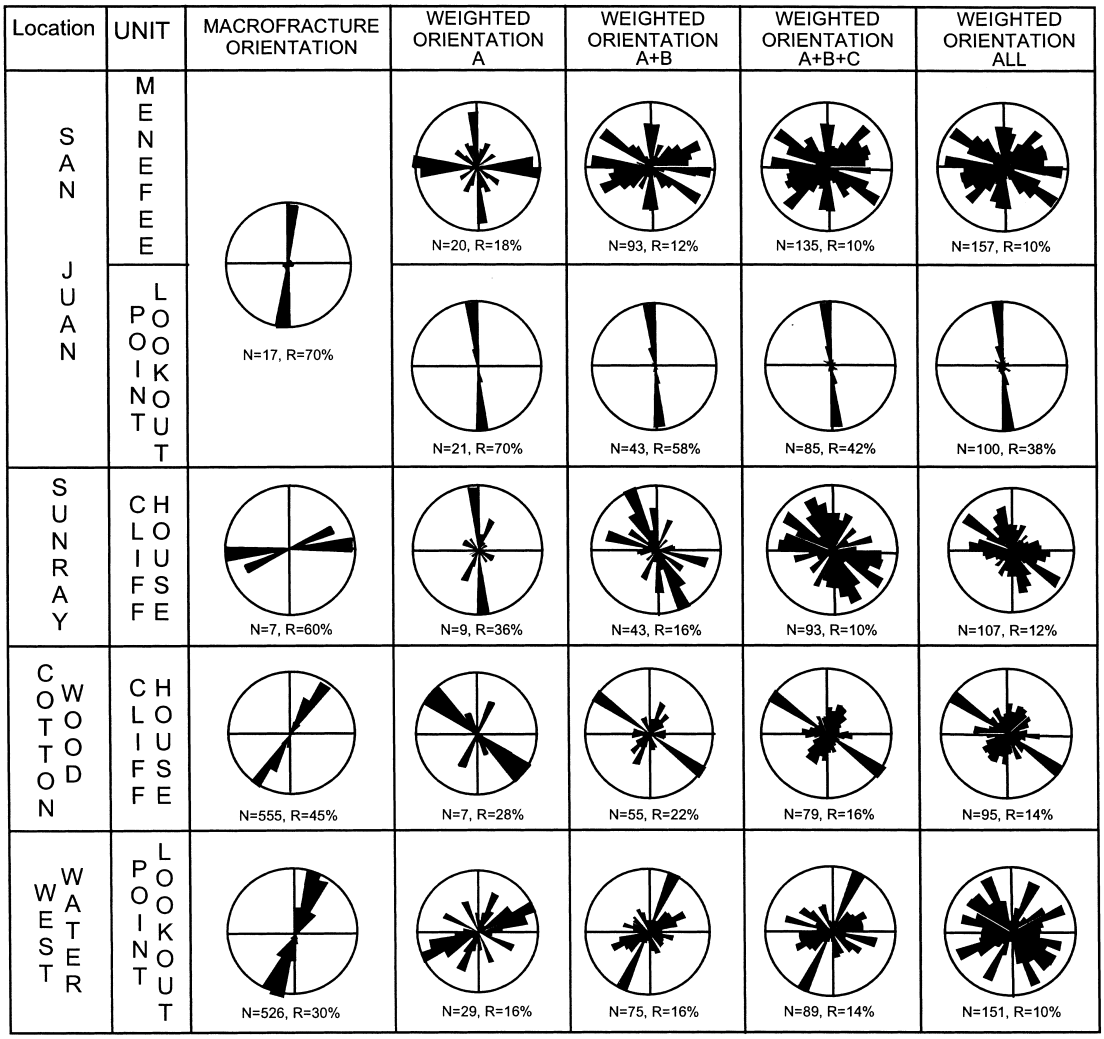

Fig. 7. Microfracture strike comparison with macrofracture strikes. Results for five thin sections from San Juan 32-9, Sunray H Com ♯6 wells and outcrops. All microfracture rose diagrams were weighted by fracture length. *N* and *R* are the same as in Fig. 6.

pavement are much more abundant and were only studied in the small observation area, in which some long fractures also were observed. To select the best model for the length distribution of short fractures, long fractures were excluded from consideration and an analysis of the least-squares regression errors was carried out (Fig. 9B). For the smallest fracture lengths in the data set (length < 500 mm), the correlation coefficient is highest for the exponential regression (from smallest to largest fractures), suggesting that the smallest fractures are best modeled by an exponential function. A crossover in correlation coefficients occurs at a length of 500 mm, such that the correlation coefficient is highest for the power-law regression (from largest to smallest fractures) for fractures between 500 and 2900 mm in length, suggesting that these fractures are best modeled by a power-law function.

The power laws that provide the best fits to fracture lengths on the Westwater pavement have different exponents for long and short fractures. This change in exponents at the scale of the mechanical layer thickness is corroborated by the data from long fractures in the small observation area, although the number of these fractures is insufficient to model with confidence. Previous analyses of analogous changes in length distributions concluded that the changes reflected a censoring bias in the sampling procedure (e.g. Baecher and Lanney, 1978; Barton and Zoback, 1992). Censoring was minimized in this experiment by studying nearly 100 long fractures within an area having dimensions more than an order of magnitude greater than the length of the longest fractures observed. Consequently, we interpret this change in power-law exponent to be a real phenomenon.

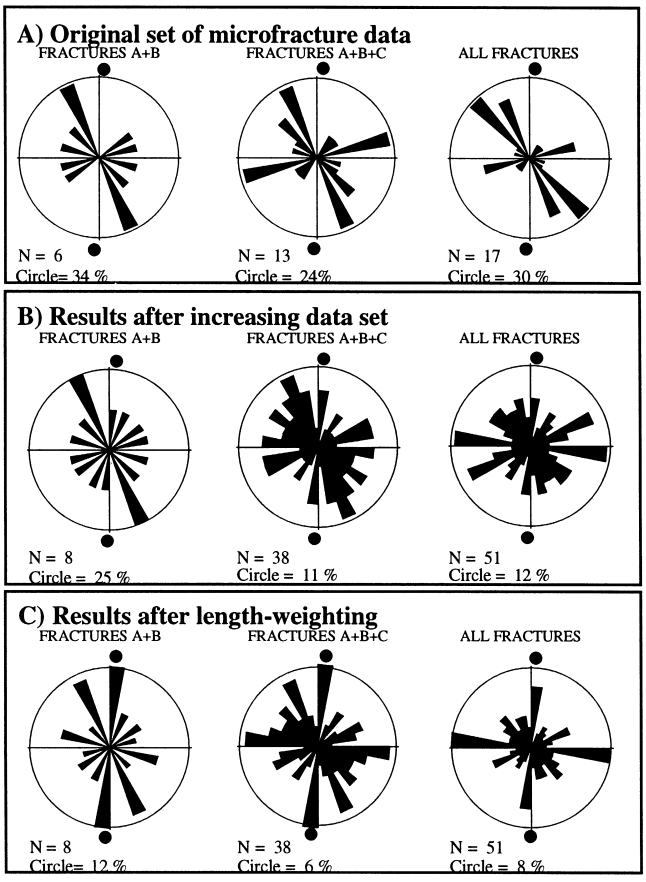

Fig. 8. Microfracture orientation sensitivity analysis, Riddle D LS 4A well. Black circles outside the rose diagrams indicate the strike of the macrofractures at the depth of the sample. *N* is the same as in Fig. 6.

In order to confirm these results, a second set of data was recorded from the Cottonwood pavement. In this case the mechanical layer is thinner (1.5 m) and the collection of macrofracture data in two different size observation areas was unnecessary. A single area of about 2000 m^2 was selected to measure all visible macrofractures. Long fractures are again well modeled by a power law (Fig. 10). Although short fractures greater than 200 mm in length are well modeled by a power law having a smaller exponent than that of the long fractures, an exponential function provides comparable or marginally better correlation coefficients. Consequently, in this case it is unclear what the best interpretation is for the short fractures; either a change in power-law scaling occurs or power-law scaling breaks down at the scale of mechanical layer thickness.

4.5.2. Prediction of macrofracture frequency using microfracture frequency

Power-law regressions to the microfracture length distributions for the Westwater and Cottonwood pavements yield extrapolations that reasonably predict the observed frequencies of macrofracture lengths in these pavements (Fig. 11). In contrast, exponential regressions to the microfracture length distributions grossly under-predict the observed macrofracture lengths, suggesting that either the exponential model is an invalid mathematical description of the fracture system, or that the micro- and macrofracture populations are not expressions of the same fracture system. For example, the exponential model fit to the microfractures of the Cottonwood pavement predicts only one fracture, one millimeter long or longer, in an area of approximately 10,000 m^2, which is in flagrant contradiction with the observations from the outcrops. An estimate using a power-law model predicts one fracture 4 m long or greater in an area of approximately 1000 m^2, which matches the observations.

The exponent of the power-law fit to the microfracture size distributions from the pavements studied (-1.98 and -1.94) are considerably more negative than the exponents obtained for the 'short' macrofractures in the same pavements (-1.25 and -1.26, respectively). Several explanations might account for

these differences; the possible causes include incorrect determination of fracture terminations in outcrop, fracture exposure limitations due to outcrop conditions (weathering, lichen patches, soil or vegetation) and/or misleading results arising from the error analysis for the macrofracture length population. The extrapolation of the power-law regression to the 'short' macrofractures of Westwater pavement to the microscale predicts only one microfracture 10 μm long or longer in an area of approximately 10 mm^2, which is inconsistent with observations and suggests that the model for 'short' macrofractures is suspect. An alternative explanation for this discrepancy could be that most of the microfractures observed under the SEM-CL are not related to the macrofractures observed in the pavements.

We prefer to interpret that the power-law fit to the macrofractures is poor, most probably due to inadequate determination of fracture terminations and limitations of fracture exposure in the field. The relationships between the microfractures and the macrofractures studied, based on the similarities of micro- and macrofracture orientations and cementation, support the satisfactory quantitative relations between lengths provided by the power-law regression to the microfractures. This result suggests that a prediction of macrofracture frequency might be possible using microfracture frequency data. Additionally, this result suggests that there are no major changes in the fracture length distributions from the microscale (at least above the grain scale) to the macroscale (at least below the scale of mechanical layer thickness), and that these two scales of fractures are only two different size fractions of a single fracture system.

Fracture height data collected along Westwater Springs Canyon were also compared with microfracture size distributions from pavement samples. A direct comparison of the microfracture length and macrofracture height distributions is possible if we assume that the microfractures are penny shaped, namely that fracture lengths and heights are comparable. The power-law relationship obtained from the microfracture length population predicts the fracture heights reasonably well in this case (Fig. 12).

4.5.3. One-dimensional–two-dimensional fracture size distribution conversions

The scanline data obtained from the small area of

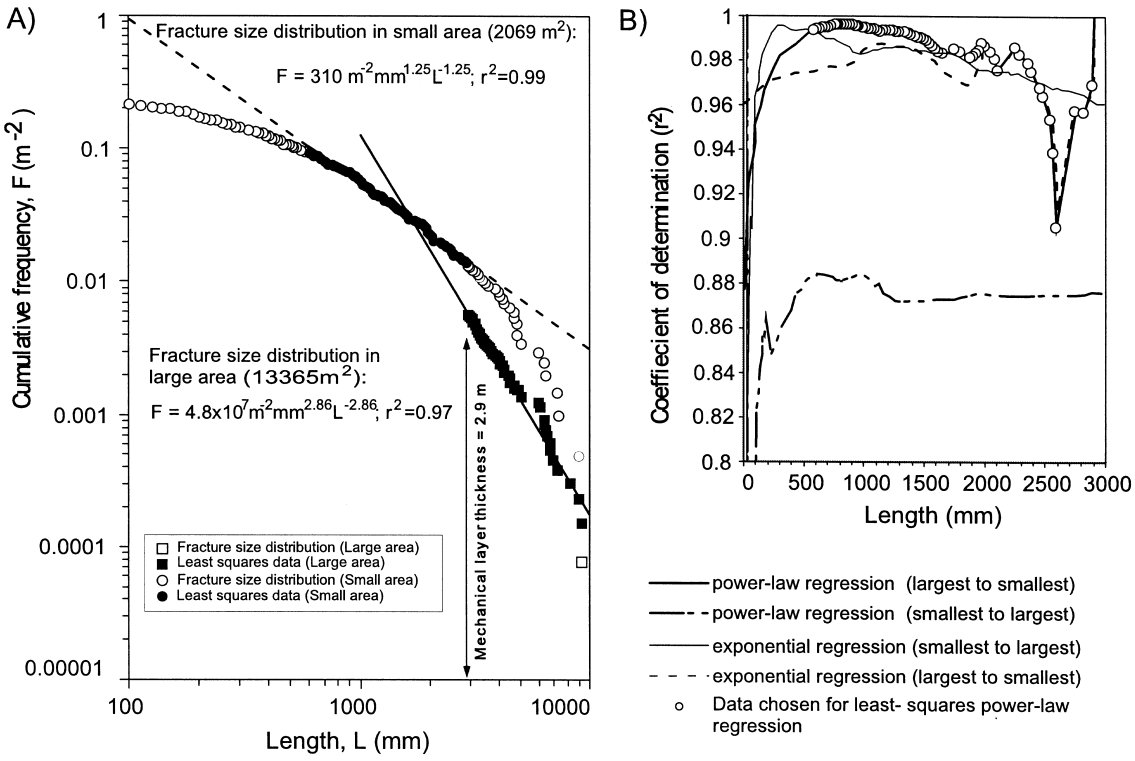

Fig. 9. Effect of mechanical layer on fracture size distributions, Westwater pavement. Least-squares regressions have been fit to the segments of the fracture size distributions that show the highest correlation coefficients (A). The dashed line represents the power-law regression to fractures shorter than the mechanical layer thickness based on the error analysis (B), and the continuous line is the power-law regression to fractures longer than the mechanical layer thickness from the large observation area. The differences obtained in the power-law distributions for fractures longer and shorter than the thickness of the mechanical layer suggest that the mechanical layer plays a role in the observed fracture size distributions.

Westwater pavement can be used to validate theoretical techniques for conversion between one- and two-dimensional distributions (Fig. 13). The preferred least-squares power-law regression extrapolated from the two-dimensional cumulative frequency distribution of microfracture lengths was used to calculate predicted one-dimensional length distributions of the macrofractures using Marrett's (1996) approach.

Sampling topology introduces artifacts when fractures shorter than the thickness of the mechanical layer are sampled in one-dimensional or two-dimensional sampling domains. Two- or one-dimensional sampling will typically under-sample these fractures with respect to their true abundance in the rock volume. Fractures shorter than the mechanical layer thickness are organized such that their fracture-size distribution follows the predicted one-dimensional model. The predicted distribution for long fractures, sampled along scanlines, has an exponent similar to that of the power-law regression calculated from the microfractures. This artifact is produced because the probability to sample a long fracture in a layer-parallel sample line is the fracture length divided by pavement width, whereas the probability to sample a small fracture in a layer-parallel sample plane along the pavement is fracture height (~length) divided by pavement thickness. In both cases the apparent frequency distributions will have an exponent equal to one plus the (negative) exponent of the three-dimensional frequency distribution of fracture lengths. The result is an apparent two-dimensional sampling for long fractures.

5. Discussion

5.1. Fracture-fill volume

Although micro- and macrofractures share the temporal sequence of cementation, differences in the degree of occlusion between the micro- and macrofractures suggest that microfractures do not provide a simple proxy for the degree of occlusion of macrofractures. Microfractures tend to be more readily filled by cement than macrofractures, possibly because of their impurity-free fracture walls and greater surface area to volume ratios. Additionally, microfractures in the sandstones studied tend to be preferentially filled with quartz whereas carbonate cement (relatively late in petrogenesis) is found almost exclusively in the macrofractures. The largest fractures not only have the largest apertures, and consequently permeability, but they

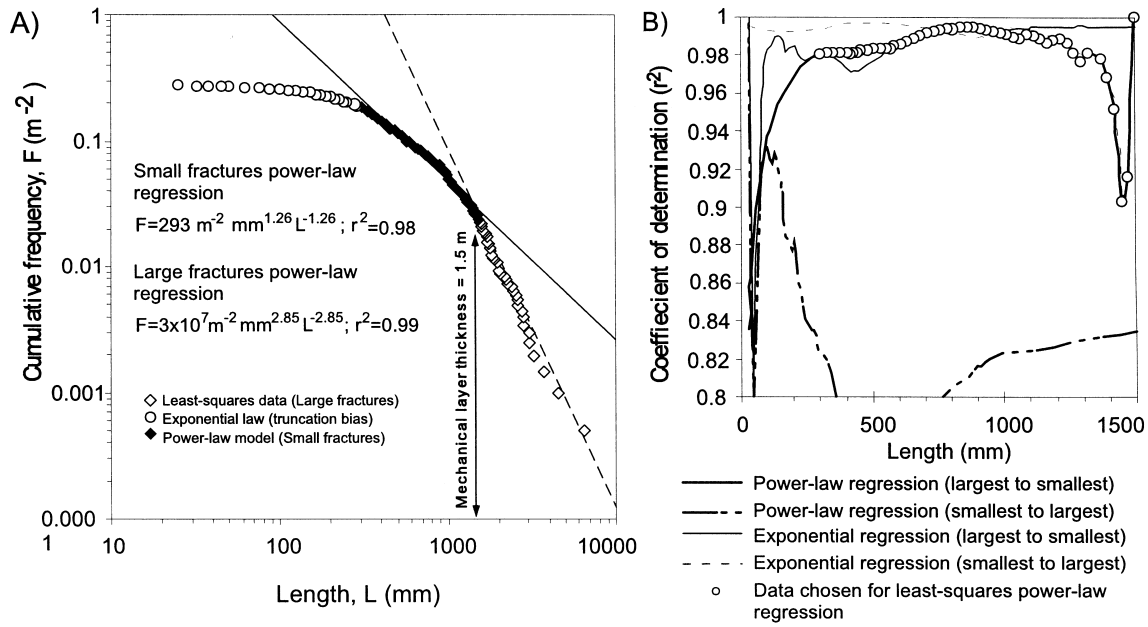

Fig. 10. Effect of mechanical layer on fracture length distributions, Cottonwood pavement. Assuming that different power-law models are valid for fractures smaller and larger than the thickness of the mechanical layer, these results suggest that the thickness of the mechanical layer has an effect on the observed fracture size distribution. The bold continuous line in (A) represents the power-law regression to the fractures shorter than the mechanical layer thickness based on the error analysis on (B). The dashed line represents the power-law regression to fractures longer than the mechanical layer thickness. The surface area of the sampling domain is 2034 m^2.

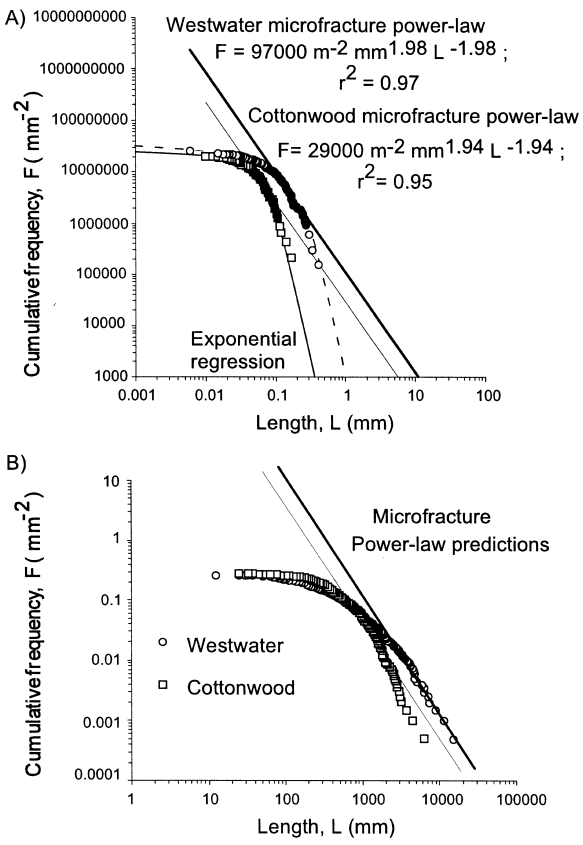

Fig. 11. Macrofracture frequency prediction using microfracture frequency data, Westwater (circles) and Cottonwood (squares) pavements. Filled symbols in microfracture distributions indicate the data used to obtain the least squares regression lines. These parts of the microfracture length distributions are best modeled using power-laws. The predicted macrofracture frequencies are close to the observed macrofracture frequencies in the pavements. Exponential laws (dashed lines) derived from the microfracture length distributions predict unreasonably low macrofracture frequencies, which do not match with the observations.

also are the most likely to remain at least partly open, increasing their importance as conduits for fluid flow.

5.2. Fracture orientation

Several geologic processes can generate microfractures in sandstones but only some of these processes produce macrofractures. Laubach (1997) provided a comprehensive discussion of microfracture morphology and origin. Microfracture orientation analyses in the Mesaverde Group sandstones suggests that transgranular and transcement microfractures have the highest suitability as proxies of macrofractures. These microfractures can show significant variations in orientation along their traces due to the heterogeneity of sandstones at the microscopic scale. Typically, as they grow longer, they tend to maintain a regular average propagation direction that reproduces the orientation of the macrofractures.

A high level of complexity characterizes microfracture orientations in the Mesaverde Group sandstones. This complexity in part reflects the material heterogeneity of the sandstones at the microscopic scale and the tectonic history that affected these rocks. However, comparison of microfracture and macrofracture strikes in areas dominated by one set of macrofractures indicates that it is feasible to predict macrofracture orientation using microfracture orientation data from properly oriented samples. The amount of data necessary to reveal the signal of the macrofractures is a function of the geologic history of the rock, the microfracture frequency, and the recognition of which microfractures were generated by the processes that produced macrofractures.

5.3. Fracture connectivity

Most previous work on fracture connectivity and fluid flow derives from percolation theory, but no quantification of the connectivity is obtained with this technique (Lee and Farmer, 1993). In our work, a semiquantitative approach has been taken to evaluate fracture connectivity. This approach takes into account the proportion of fractures connected in the network and the way they are connected, but does not solve the scale dependency problem of fracture connectivity (Laubach, 1992). However, it does allow comparison

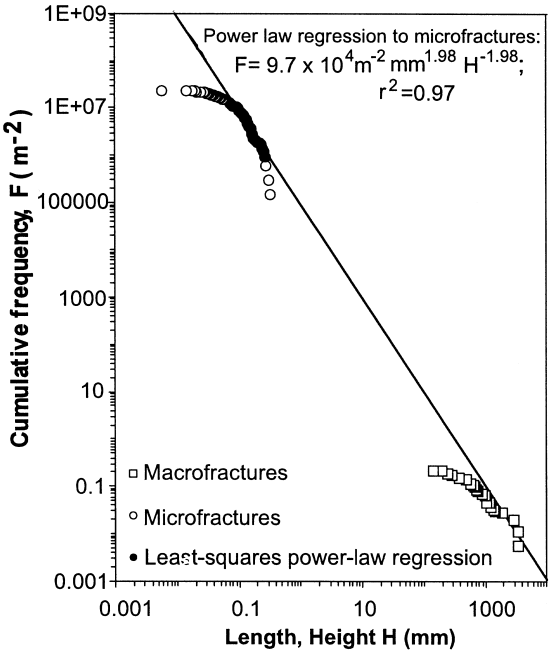

Fig. 12. Fracture height frequency prediction, Westwater Springs Canyon. The parameters of the power-law fit to the microfracture size distribution in Fig. 11 also give a reasonable prediction of the macrofracture height distribution at least up to the scale of the bed thickness.

and contrast of fracture network connectivity at a selected observation scale. Additionally, it provides meaningful reference parameters to be used in fracture-mechanics and fluid-flow models that attempt to simulate real fracture networks.

This and other methods proposed in the literature (Robinson, 1983; Rouleau and Gale, 1985; La Pointe, 1988; Zhang et al., 1992) ignore the effects that cementation and dissolution can have on fracture connectivity. At present, no studies of these effects on fracture connectivity have been carried out. Useful evaluation of fracture connectivity for fluid-flow applications requires an understanding of the volume of mineral fill in the fractures and its variations through different scales of observation. For example, small fractures or narrow connections might be preferentially filled. In such cases geometric linkage is not equivalent to linkage of fracture porosity.

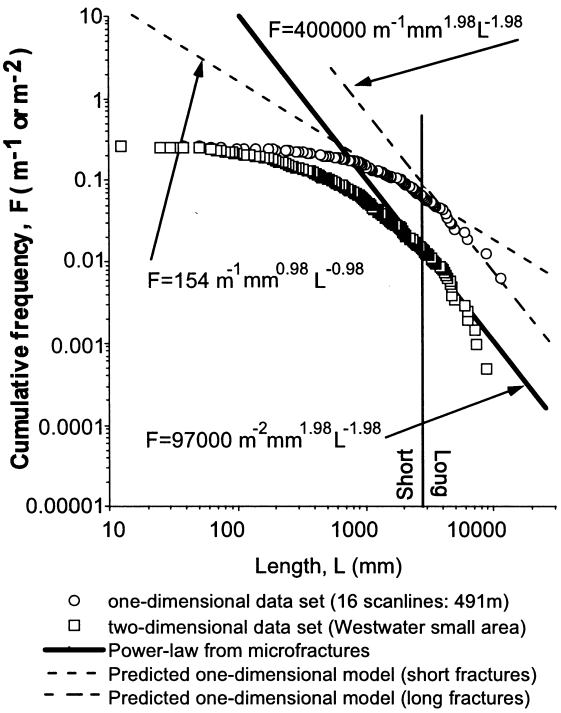

Fig. 13. Test of two-dimensional–one-dimensional sampling domain conversion, Westwater pavement. The one-dimensional distribution predicted from using formulas in Marrett (1996) adequately predicts the smallest fracture sizes from scanlines. According to Marrett (1996) the exponent of the two-dimensional power-law distribution (e_S) and the one-dimensional power-law distribution (e_T) follow the relationship: $e_S = e_T + 1$. The coefficients can be calculated using the formula: $h_S e_S = 4\ h_T e_T/\pi$; where h_S and h_T are the coefficients of the two-dimensional and one-dimensional power laws, respectively. The slope of the size distribution for medium-size fractures sampled along the scanlines is similar to the slope of the two-dimensional distribution because the probability of sampling medium-size fractures with fracture-perpendicular scanlines repeatedly crossing the study area is similar to sampling the fractures in the two-dimensional observation area.

The microfractures in sandstones of the Mesaverde Group are in almost all cases completely filled with cement and do not contribute to present hydrodynamic fracture connectivity. In these circumstances, connectivity can be ignored below the scale at which the fractures are open.

5.4. Fracture size distributions

The characterization of macrofracture size distribution and frequency in the subsurface is even more difficult than the characterization of macrofracture orientation, because a large and complete inventory of the fractures is necessary. For economically important large fractures such an inventory is not possible using current technology, except in special cases.

The results obtained from fracture networks in the Mesaverde Group sandstones indicate that the best model for fracture size distributions is a power-law model, particularly at the scales of observation where fracture sizes are best controlled. Microfracture length distributions are closely related to macrofracture length distributions. These results justify using microfracture lengths to predict macrofracture length and frequency in the subsurface.

Different sampling topologies produce different exponents of power-law fracture-size distributions (Marrett, 1996). Independent results obtained in a pavement of Mesaverde Group sandstones demonstrate this effect and were confirmed on a second pavement using more conventional methods of fracture data collection. Surface mapping results in a three-dimensional sampling of fractures longer than the mechanical layer thickness and a two-dimensional sampling of shorter fractures. In other words, fractures shorter than the thickness of the bed are undersampled (relative to the number that exists in three dimensions) in bed-parallel exposures, whereas all fractures longer than the thickness of the layer are sampled in the same two-dimensional observation area.

Power-law regression to the microfractures adequately predicts the frequency of macrofractures in both pavements studied up to the scale of the thickness of the mechanical layer. Fractures longer than the thickness of the mechanical layer are artificially sampled in pseudo-three-dimensional domains and their frequencies are not directly comparable to the frequencies of two-dimensionally sampled microfractures, but a conversion from one to the other is straightforward (Marrett, 1996), provided that the layer thickness is known.

6. Conclusions

This study evaluated the use of microfracture data to predict macrofracture attributes and found that useful information can be reliably derived using this approach. Systematic analysis of abundant microfractures in small pieces of rock overcomes the severe limitations of acquiring subsurface macrofracture data.

Tests carried out on samples from Mesaverde Group sandstones, where macrofracture orientation and frequency are known, showed that in some cases the predictive value of the microfractures is high (i.e. microfractures are an expression of the macrofracture system at the microscopic scale). For example, fracture orientation remains constant through different scales in many cases.

Analysis of outcrop data indicates that extrapolations of fracture frequencies from the microscopic scale to the macroscopic scale are possible and reliable at least up to the scale of mechanical layers. Experiments carried out on large Mesaverde Group sandstone exposures demonstrate that the presence of mechanical boundaries affects the fracture-size distribution obtained in two-dimensional observation areas. Typically, the size-distributions of fractures that span the mechanical layer follow power-laws of more negative exponent than followed by smaller fractures.

Given that censoring bias was specifically avoided, the observed changes in fracture scaling at the mechanical layer thickness do not appear to be artifacts. Two alternative explanations for the changes in the fracture-size distributions might be that they are related to changes in the sampling topology (Marrett, 1996) and that they are a real effect produced by the presence of the mechanical boundaries of the fractured layer (Wojtal, 1996). The effect of changes in sampling topology can be understood by conceptualizing the geometrical implications of sampling different fracture sizes in a mechanically stratified volume of rock. Although the data collected cannot directly support the second effect, common observations support the idea that mechanical boundaries affect fracture growth; for example, bed-scale fractures commonly terminate at bed planes.

Fractures longer than the thickness of mechanical layering show a more restricted range of lengths than smaller fractures. Once the dimension of a mechanical layer is determined, a theoretical approach to calculate fracture permeability can be addressed knowing that the permeability is fundamentally controlled by the largest fractures in a reservoir (Marrett, 1996).

The quantification of fracture connectivity and the evaluation of fracture opening/cementation relative timing can help to evaluate the capacity of a particular fracture system to conduct fluid and drain fluids stored in the rock matrix adequately. In this study, the characterization of fracture connectivity was approached using new concepts. The probabilities of a fracture being isolated, singly connected or fully connected can be calculated from a fracture map at a given scale. These parameters take into account the geometrical characteristics of the fracture network and complement previous approaches to quantify fracture connectivity (Robinson, 1983). The connectivity of the fracture network can be characterized and compared with results from fluid-flow and mechanical models.

Subsurface sandstones of the Mesaverde Group in two of the wells studied show important volumes of prekinematic cements and small volumes of postkinematic cements, indicating that fractures in the sampled intervals should be open. The volume of postkinematic cement in outcrop samples is greater than in subsurface samples, possibly due to regional variations in diagenetic history and/or fracture timing.

Microfractures are mostly filled with cement and do not contribute to porosity and permeability in the reservoir. The proportions of cement phases filling the fractures varies with fracture scale in these rocks. This observation has implications for the understanding of scale-dependent fluid flow and prediction of fracture openness using microscopic observations.

Acknowledgements

This work was supported by BDM-Oklahoma grant G4S51732 (U.S. Department of Energy contract DE-AC22-94PC91008), Petroleos de Venezuela, and the industrial associates of the Fracture Research and Application Consortium (ARCO Exploration and Production, Chevron Petroleum Technology Co., Conoco Inc., Exxon Production Research, Maxus Energy Corp., Mobil Technology Co., Sanchez Oil and Gas, Tom Brown Inc., Union Pacific Resources). The authors thank Steve Laubach for comments and discussions throughout the development of this research work, and Robert Reed, Kitty Milliken and Sigrid Clift for their help with the SEM-CL.

References

Baecher, G.B., Lanney, N.A., Einstein, H.H., 1977. Statistical description of rock properties and sampling. 18th US Symposium on Rock Mechanics 5C1, 1–8.

Baecher, G.B., Lanney, N.A., 1978. Trace length biases in joint surveys. Proceedings, Symposium on Rock Mechanics 19, 56–65.

Barton, C.A., Zoback, M.D., 1992. Self-similar distribution and properties of macroscopic fractures at depth in crystalline rock in the Cajon Pass scientific drill hole. Journal of Geophysical Research 97, 5181–5200.

Belfield, W.C., Sovich, J.P., 1995. Fracture statistics from horizontal wellbores. Journal of Canadian Petroleum Technology 34, 47–50.

Bond, W.A. 1984. Application of Lopatin's method to determine

burial history, evolution of the geothermal gradient, and timing of hydrocarbon generation in Cretaceous source rocks in the San Juan basin, northwestern New Mexico and southwestern Colorado. In: Woodward, J., Meissner, F.F., Clayton, J.L. (Eds.), Hydrocarbon Source Rocks of the Greater Rocky Mountain region. Rocky Mountain Association of Geologists, pp. 433–448.

Clark, M.B., Brantley, S.L., Fisher, D.M., 1995. Power-law vein thickness distributions and positive feedback in vein growth. Geology 23, 975–978.

Condon, S.M. 1988. Joint patterns on the northwest side of the San Juan basin (Southern Ute Indian Reservation), southwest Colorado. In: Fassett, J.E. (Ed.), Coal-Bed Methane in San Juan Basin, Colorado and New Mexico. Rocky Mountain Association of Geologists, pp. 61–68.

Condon, S.M., 1989. Fracture studies on the eastern side of the Southern Ute Indian Reservation. U.S. Geological Survey Administrative Report, BIA-19-II-E.

Corbett, K., Friedman, M., Spang, J., 1987. Fracture development and mechanical stratigraphy of Austin Chalk, Texas. American Association of Petroleum Geologists 71, 17–28.

Dart, S.W. 1992. Evaluation of San Juan basin fractured reservoirs from surface data. In: Schmoker, J.K., Coalson, E.B., Brown, C.A. (Eds.), Geological Studies Relevant to Horizontal Drilling: Examples from Western North America. Rocky Mountain Association of Geologists, pp. 95–114.

Folk, R.L., 1980. Petrology of Sedimentary Rocks. Hemphill Publishing Company, Austin.

Gillespie, P.A., Howard, C.B., Walsh, J.J., Watterson, J., 1993. Measurement and characterization of spatial distributions of fractures. Tectonophysics 226, 113–141.

Gorham, F.D., Woodward, L.A., Callender, J.F., Greer, A.R., 1979. Fractures in Cretaceous rocks from selected areas of San Juan basin, New Mexico, exploration implications. American Association of Petroleum Geologists 63, 598–607.

Gross, M.R., 1993. The origin and spacing of cross joints: Examples from the Monterrey Formation, Santa Barbara coastline, California. Journal of Structural Geology 15, 737–751.

Gross, M.R., Engelder, T., 1995. Strain accommodated by brittle failure in adjacent units of the Monterey Formation, U.S.A.: Scale effects and evidence for uniform displacement boundary conditions. Journal of Structural Geology 17, 1303–1318.

Gudmundsson, A., 1987. Geometry, formation and development of tectonic fractures on the Reykjanes peninsula, southwest Iceland. Tectonophysics 139, 295–308.

Hatton, C.G., Main, I.G., Meredith, P.G., 1994. Non universal scaling of fracture length and opening displacement. Nature 367, 160–162.

Heffer, K.J., Bevan, T.G., 1990. Scaling relationships and natural fractures: data, theory and applications. Society of Petroleum Engineers 20981, 367–376.

Helgeson, D., Aydin, A., 1991. Characteristics of joint propagation across layer interfaces in sedimentary rocks. Journal of Structural Geology 13, 897–911.

Hollenshead, C.T., Pritchard, R.L. 1961. Geometry of producing Mesaverde sandstones, San Juan basin. In: Peterson, J.A., Osmond, J.C. (Eds.), Geometry of Sandstone Bodies — A Symposium. American Association of Petroleum Geologists, pp. 98–118.

Huffman, A.C. Jr, Condon, S.M., 1993. Stratigraphy, structure and paleogeography of Pennsylvanian and Permian rocks, San Juan basin and adjacent areas, Utah, Colorado, Arizona, and New Mexico; US Geological Survey, 1–44.

Johnston, J.D., McCaffrey, K.J.W., 1996. Fractal geometries of vein systems and the variation of scaling relationships with mechanism. Journal of Structural Geology 18, 349–358.

Kelley, V.C., Clinton, N.J., 1960. Fracture systems and tectonic elements of the Colorado Plateau. New Mexico University Publications in Geology 6, New Mexico University Press.

Kulander, B.R., Dean, S.L., Ward, B.J. Jr, 1990. Fractured core analysis. Interpretation, logging, and use of natural and induced fractures in core. American Association of Petroleum Geologists, Methods in Exploration Series No. 8, Tulsa.

La Pointe, P.R., 1988. A method to characterize fracture density and connectivity through fractal geometry. International Journal of Rock Mechanics, Mining Sciences and Geomechanics 25, 421–429.

Laslett, G.M., 1982. Censoring and edge effects in areal and line Transects sampling of rock joint traces. Mathematical Geology 14, 125–140.

Laubach, S.E., 1988. Subsurface fractures and their relationship to stress history in east Texas basin sandstone. Tectonophysics 156, 495–503.

Laubach, S.E. 1992. Fracture networks in selected Cretaceous sandstones of the Green River and San Juan basins, Wyoming, New Mexico and Colorado. In: Schmoker, J.W., Coalson, E.B., Brown, C.A. (Eds.), Geological Studies Relevant to Horizontal Drilling: Examples from Western North America. Rocky Mountain Association of Geologists, pp. 115–127.

Laubach, S.E., 1997. A method to detect natural fracture strike in sandstones. American Association of Petroleum Geologists 81, 604–623.

Laubach, S.E., Tremain, C.M. 1991. Regional coal fracture patterns and coalbed methane development. In: Roegiers, J.C. (Ed.), Rock Mechanics as a Multidisciplinary Science Balkema, pp. 851–859.

Laubach, S.E., Hentz, T.F., Johns, M.K., Baek, H., Clift, S.J., 1995. Using diagenesis information to augment fracture analysis. Topical report ♯GRI-94/0455. Bureau of Economic Geology, The University of Texas, Austin.

Laubach, S.E., Milliken, K.L. 1996. New fracture characterization methods for siliciclastic rocks. In: Hassani, M.F., Mitri, H. (Eds.), Proceedings 2nd North American Rock Mechanics Symposium. Balkema, pp. 1209–1213.

Lee, C., Farmer, I., 1993. Fluid Flow in Discontinuous Rocks. Chapman and Hall, London.

Marrett, R., Allmendinger, R.W., 1991. Estimates of strain due to brittle faulting: sampling of fault populations. Journal of Structural Geology 13, 735–738.

Marrett, R., 1996. Aggregate properties of fracture populations. Journal of Structural Geology 18, 169–178.

Marrett, R. 1997. Permeability, porosity, and shear-wave anisotropy from scaling of open fracture populations. In: Hoak, T.E., Klawitter, A.L., Blomquist, P.K. (Eds.), Fractured Reservoirs: Characterization and Modeling Guidebook. Rocky Mountain Association of Geologists, pp. 217–226.

Marrett, R., Laubach, S.E., 1997. Diagenetic controls on fracture permeability and sealing. International Journal of Rock Mechanics and Mining Sciences 34. Paper 204.

Milliken, K.L., 1994. Cathodoluminescent textures and the origin of quartz silt in Oligocene mudrocks, south Texas. Journal of Sedimentary Research A64, 567–571.

Olson, J.E., 1993. Joint pattern development, effects of subcritical crack growth and mechanical crack interaction. Journal of Geophysical Research 98, 12251–12265.

Ortega, O., 1997. Prediction of macrofracture properties using microfracture information, Mesaverde Group sandstones, San Juan basin, New Mexico. MSc. Thesis, University of Texas at Austin.

Pickering, G., Bull, J.M., Sanderson, D.J., 1995. Sampling power-law distributions. Tectonophysics 248, 1–20.

Robinson, P.C., 1983. Connectivity of fractured systems — A percolation theory approach. Journal of Physics. A: Mathematical and General 17, 605–614.

Rouleau, A., Gale, J.E., 1985. Statistical characterization of the fracture system in the Stripa granite, Sweden. International Journal

of Rock Mechanics, Mining Sciences and Geomechanics 22, 353–367.

Sanderson, D.J., Roberts, S., Gumiel, P., 1994. A fractal relationship between vein thickness and gold grade in drill core from La Codosera, Spain. Economic Geology 89, 168–173.

Snow, D.T., 1970. The frequency and apertures of fractures in rock. International Journal of Rock Mechanics and Mining Sciences 7, 23–40.

Weir, G., 1996. Petrophysical Characterization of the Tight Gas Production in the Mesaverde Group of the San Juan basin. Amoco, Tulsa.

Wong, T.F., Fredrich, J.T., Gwanmesia, G.D., 1989. Crack aperture statistics and pore space fractal geometry of Westerly granite and Rutland quartzite: Implications for an elastic contact model of rock compressibility. Journal of Geophysical Research 94, 10267–10278.

Wojtal, S.F., 1994. Fault scaling laws and the temporal evolution of fault systems. In: Brandon, M.T., Henderson, J.R., Means, W.D., Peterson, S.R. (Eds.), Applications of Strain; from Microstructures to Orogenic Belts, Journal of Structural Geology, 16, pp. 603–612.

Wojtal, S.F., 1996. Changes in fault displacement populations correlated to linkage between faults. Journal of Structural Geology 18, 265–280.

Zhang, X., Harkness, R.M., Last, N.C., 1992. Evaluation of connectivity characteristics of naturally jointed rock masses. Engineering Geology 33, 11–30.